

A 10-year climatology of vertical properties of most active convective clouds over the Indian regions using TRMM PR

Shailendra Kumar¹

Received: 6 February 2014 / Accepted: 8 September 2015 / Published online: 28 September 2015
© Springer-Verlag Wien 2015

Abstract Vertical distribution of hydrometeors in the most intense convective clouds over the Indian region during the summer monsoon season (JJAS) is described for ten climatologically important areas. Tropical Rainfall Measuring Mission Precipitation Radar (TRMM PR) 3D radar reflectivity data is used in the present study for 10 years (2001–2010). The study constructs a convective cloud cell based on reflectivity thresholds, known as most intense convective cloud. The cloud cells are formed by taking the maximum reflectivity (Z_e) at each altitude in the convective area with at least one radar pixel containing reflectivity of 40 dBZ or more. TRMM 2A23 data was used to eliminate the stratiform clouds from our analyses. The Vertical structure of convective clouds were studied over the east and west coast of India, and observation shows that the east coast consists of a higher frequency of convective clouds with high reflectivity values in average vertical profiles. It is observed that over the northeastern parts of the Indian subcontinent, ~30 % of convective cells extend beyond 15-km height whereas it is only ~4 % over the central Bay of Bengal. Over the Western Ghats, ~13 % of the cells have their tops below the freezing level, i.e. warm clouds do give heavy rain here. The regional differences in the vertical profile are high between the 5- and 12-km altitude. Most intense convective cells (MICCs) with a cloud top height more than 10 and 15 km show different characteristics, and the

Western Ghats shows the most intense average vertical profile. Above 12 km, the western coast shows increased reflectivity value. Convective intensity is higher over the land-dominated areas for the cloud cells and decreases when we restrict the cloud cells to a certain altitude.

1 Introduction

The tropical cumulonimbus clouds (Cb), which are also classified as ‘hot towers’ (Riehl 1979), play an important role in Earth’s water and energy cycle and are responsible for atmospheric circulation (Charney 1969; Holton 2004). Maximum contribution to vertical transportation of energy comes from Cb clouds (Riehl 1979) and also feed hydrometeors to stratiform regions of mesoscale convective systems (MCSs, e.g. Houze 1989). The Tropical Rainfall Measuring Mission Precipitation Radar (TRMM PR, henceforth) provides the volumetric data of reflectivity (in dBZ) since its launch date (i.e. December 1997), and it consists of large time series data for understanding precipitating cloud systems (Kummerow et al. 1998, 2000).

TRMM PR is used with other on-board sensors, such as the TRMM microwave imager (TMI), to study the properties of precipitating cloud systems. ‘TRMM precipitation features (PFs)’ contain the data from different sensors mounted on the TRMM satellite (Nesbitt et al. 2000). These PFs are used for extracting the properties of tropical cloud systems (Nesbitt et al. 2006; Liu et al. 2008; Liu et al. 2012; Xu and Zipser 2012). Deep convective clouds export water from the troposphere to the stratosphere (e.g. Simpson et al. 1998) and ~5 % of clouds are involved in this process (Alcala and Dessler 2002). Inter-comparison between continental and oceanic cloud system is done by using the TRMM data (Nesbitt et al. 2000; Toracinta et al. 2002). Generally, continental areas exhibit a higher fraction of deep convective clouds and higher

Electronic supplementary material The online version of this article (doi:10.1007/s00704-015-1641-5) contains supplementary material, which is available to authorized users.

✉ Shailendra Kumar
shailendra@caos.iisc.ernet.in

¹ Centre for Atmospheric and Oceanic Sciences, Indian Institute of Science, Bangalore 560012, India

reflectivity (Z_e) values compared to oceanic cloud systems. Central Africa, Argentina and India (land areas) show deeper and horizontally more extensive PFs compared to oceans (Liu et al. 2007). Geographic locations strongly affect the properties of deep convective clouds, but warm precipitation does not show regional differences in size and intensity features (Liu et al. 2008). Warm clouds contribute 20 and 7.5 % to the total precipitation over tropical oceans and land (Liu et al. 2008), respectively. Xu and Zipser (2012) reveal that a storm with $Z_e \geq 40$ dBZ above 6 km is four times higher over land (40 %) compared to the ocean (10 %). Other significant properties of precipitating clouds such as diurnal variation (e.g. Takayabu 2002) and spatial distribution (Hirose and Nakamura 2005) have also been studied using the TRMM PR in the tropics.

TRMM PR reflectivity values are used to separate the deep and wide convective echoes (Houze et al. 2007; Romatschke et al. 2010; Medina et al. 2010; Romatschke and Houze 2011a). Deep convective echoes are defined as the area of reflectivity higher than 40 dBZ above 10 km, whereas wide intense convective echoes consist of the area of $Z_e \geq 40$ dBZ more than 1000 km² at any altitude. The western Himalayan foothills show small organized convective systems, whereas the eastern Himalayan foothills have a large size of stratiform precipitation (Houze et al. 2007; Romatschke et al. 2010). Romatschke and Houze (2011a) observed that premonsoon rain is more convective in nature, and south Asian regions show similarity in cloud systems during premonsoon and monsoon seasons (Romatschke and Houze 2011b). Saikranthi et al. (2014) investigated the convective and stratiform precipitation characteristics over the Indian subcontinent for different seasons. All the previous studies used the minimum area or contiguous pixels to verify the convective properties of the cloud systems. TRMM PR has a high spatial resolution (5 km × 5 km), and the present study uses PR reflectivity values to identify the convective properties at high spatial resolution. Investigating 40 dBZ at a very high resolution shows the properties of convective clouds at their individual scale, as the horizontal resolution of PR coincides with the horizontal size of updrafts core (4–5 km, Lucas et al. 1994). The main aim of the present study is to find the regional differences between the most intense convective clouds, their frequency of occurrences and how the vertical profiles differ when they cross the specific altitude (such as 10 and 15 km). Which altitudes show the maximum regional differences, such as near the surface or in mixed-phase height or above the troposphere? What are the regional differences in the most intense convective cloud at the east and west side regions of India? Answers to these questions will lead to improvement in the model simulation of intense convective clouds, cumulus parameterizations, satellite rainfall algorithm and lightning probability (Xu and Zipser 2012).

The present work considers different Indian regions. The eastern side consists of the highly convective Bay of Bengal (Rao 1976), and the western side consists of the Western Ghats where orographic lifting promotes a large amount of precipitation (Fig. 1). In the Western Ghats, giant cloud condensation nuclei (GCCN) are found and studies show that the cloud condensation nuclei (CCN) plays an important role in precipitating clouds and cloud systems (Rosenfeld et al. 2008; Rosenfeld et al. 2012). Data and methodology are presented in Sections 2 and 3, respectively, where the concept of most intense convective cell (MICC) is introduced. Results are presented in Section 4 followed by discussion in Section 5. The conclusions are presented in Section 6.

2 Data

2.1 TRMM PR

The present study uses TRMM-PR 2A25, version-6, attenuation-corrected radar reflectivity factor (i.e. Z_e , Iguchi et al. 2000; Masunaga et al. 2002), which is a well-validated parameter (e.g. Iguchi et al. 2000). TRMM is a non-sunsynchronous satellite and samples the area between 38°S and 38°N several times a day (Kummerow et al. 1998, 2000). TRMM PR works in the Ku band (13.8 GHz) and has a wavelength of 2.2 cm. Horizontal and vertical resolutions of TRMM PR are ~4.3 km (~5 km since August 2001) and 0.25 km, respectively. The sensitivity of TRMM PR is 17 dBZ (18 dBZ since August 2001), and it does not detect the anvil part of MCS (Li and Schumacher 2011). Table 1 shows some characteristics of the TRMM PR. The TRMM PR provides a radar reflectivity factor (Z_e) in dBZ units ($\text{dBZ} = 10 \cdot \log_{10} Z$), where Z is expressed in $\text{mm}^6 \text{m}^{-3}$.

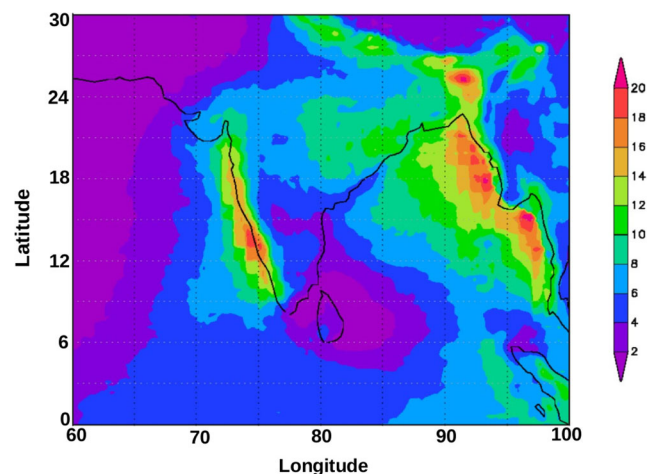


Fig. 1 Daily average rainfall derived from TRMM 3B42 rainfall product for Indian summer monsoon (JJAS) seasons. Unit in colour bar is in mm/day

Table 1 Summary of TRMM precipitation radar

Characteristics	PR specification
Frequency	13.802 GHz
Wavelength	2.2 cm
Pulse Width	1.6 μ s
Pulse repetition frequency	2776 Hz
Sensitivity	\sim 17 (18) ^a dBZ
Swath width	215 (247) ^a km
Observable range	Earth surface to 19.75 km (slant angle)
Horizontal resolution	4.3 (5.0) ^a km
Vertical resolution	0.25 km at nadir
Height	350 (402.5) ^a km

^aNumbers inside the brackets correspond to post TRMM satellite orbit height increase in August 2001

TRMM provides the vertical profile of radar reflectivity in 80 vertical levels, where the zeroth vertical level corresponds to the Earth ellipsoid. At the same time, the TRMM PR contains 49 beams, each separated by 0.71° , and provides total swath width of 247 km. TRMM 2A23 separates the radar echoes into convective and stratiform precipitation based on the vertical profile and horizontal pattern of reflectivity (Awaka et al. 2009). TRMM 2A23 data is used for the convective rain classification (Awaka et al. 2009) in the present study. TRMM 2A23 algorithm also calculates the cloud echo top height, maximum reflectivity value in the vertical profile, freezing height and width of the bright band.

2.2 Reanalysis data

Data from the National Center for Environmental prediction National Center for Atmospheric Research (NCEP-NCAR) is used at a $2.5^\circ \times 2.5^\circ$ grid (Kalnay et al. 1996) for the column water vapour, temperature and relative humidity profile.

3 Methods

3.1 Reflectivity threshold

Figure 1 shows the precipitation climatology for June–September (JJAS) from the TRMM 3B42 daily precipitation data at $0.25^\circ \times 0.25^\circ$ resolution (Huffman et al. 2007), for 2001 to 2010. The Western Ghats, Bay and Burmese mountains along the coast line of Burma show maximum rainfall. Figure 2 shows the vertical cross section of cloud system observed from the TRMM PR. A narrow region of $Z_e \geq 40$ dBZ is above the 14-km height and shows the convective cloud crossing 18 km. The horizontal size of the cloud is more than 10 km and is larger than the size of an updraft core (e.g. ~ 5 km, Zipser and Lutz 1994). Dixon and Wiener (1993) used

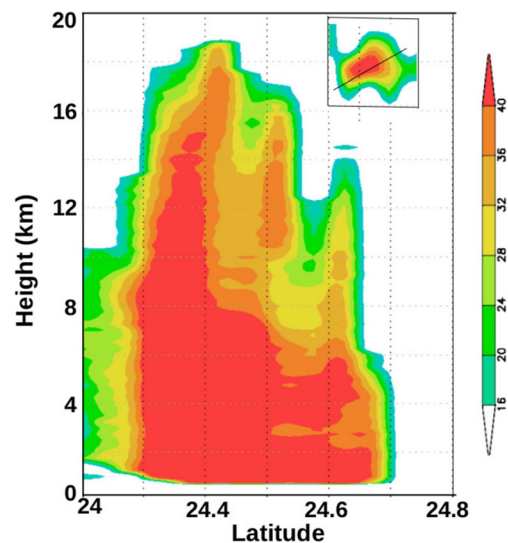
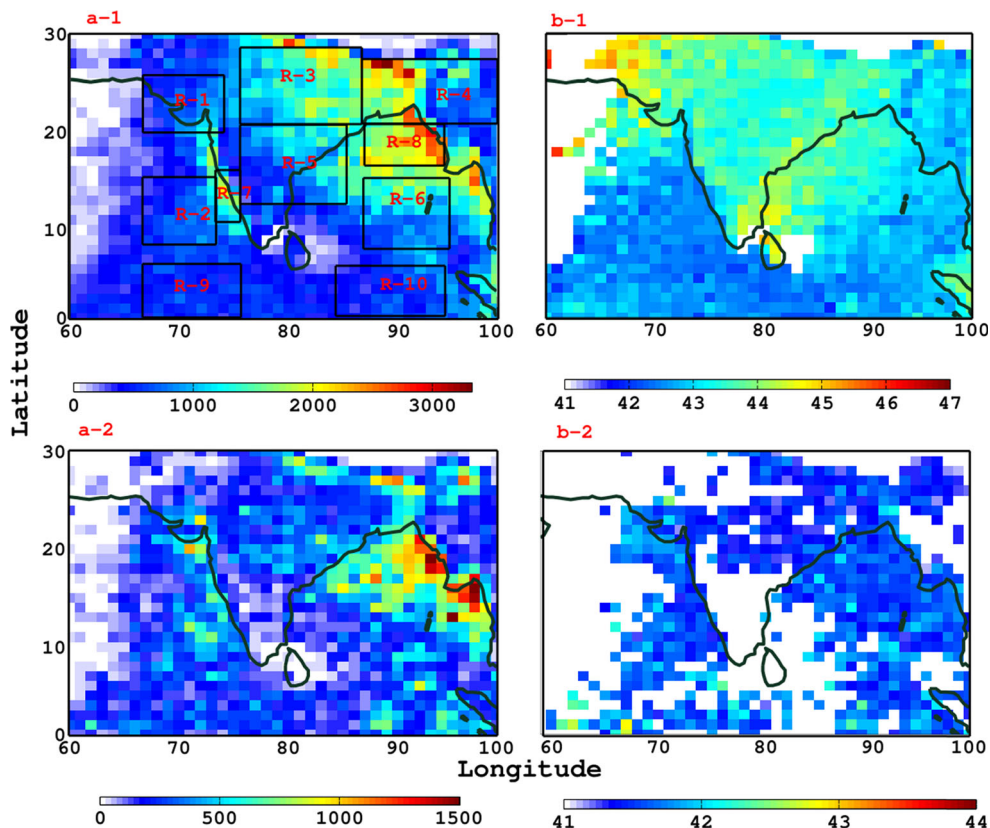


Fig. 2 Vertical section through a MCS seen by TRMM-PR on 3rd June 2003. The *inset* shows the horizontal section through the cloud system at the 3.25-km height. The *ordinate* and *abscissa* are height and latitude ($^\circ$ N), respectively. The *colour bar* on the right shows Z_e in dBZ units

the $Z_e \geq 40$ dBZ as a proxy for the individual convective cells. Steiner et al. (1995) used the $Z_e \geq 40$ dBZ for defining the convective areas in a cloud system. Forty dBZ is used as the proxy for the convective intensity (Zipser et al. 2006; Xu and Zipser 2012) and as a measure of the convective cloud (Houze et al. 2007). Deep and wide intense convective echoes have $Z_e \geq 40$ dBZ above a 10-km altitude and are more than 1000 km^2 in area (Houze et al. 2007; Romatschke et al. 2010; Romatschke and Houze 2011a, b).

Figure 3 shows the climatology of $Z_e \geq 40$ dBZ over India (60°E – 100°E and $0:30^\circ\text{N}$) within each $1^\circ \times 1^\circ$ grid box. Figure 3a-1, a-2 shows the frequency (number count) of $Z_e \geq 40$ dBZ, when Z_e is classified as convective and stratiform pixels, respectively, using TRMM 2A23 data. Numbers show that convective pixels show a higher number with $Z_e \geq 40$ dBZ, but stratiform pixels also show a significant number of $Z_e \geq 40$ dBZ ($\sim 50\%$ of the convective pixels). The Northeast India and Western Ghats show a higher fraction of convective pixels with $Z_e \geq 40$ dBZ. The Bay of Bengal and Arabian Sea show different characteristics. The north of Bay shows a higher number of convective pixels with $Z_e \geq 40$ dBZ, compared to the Arabian sea, where number pixels with $Z_e \geq 40$ dBZ exist as convective clouds. Figure 3b-1, b-2 shows the average reflectivity with $Z_e \geq 40$ dBZ for convective and stratiform pixels in each $1^\circ \times 1^\circ$ grid box, respectively. Stratiform clouds do not exceed more than 43 dBZ over the Indian subcontinent, and over most of the areas, it is well below 42 dBZ. Melting of ice into liquid below freezing level is an essential phenomenon in cloud microphysics and consists of the area of stratiform precipitation. It is important to exclude the strong melting band features from the present study. Figure 4 shows

Fig. 3 Statistics of $Z_e \geq 40$ dBZ, by using TRMM 2A23. **a-1** shows the number of convective pixels ($Z_e \geq 40$ dBZ) in each $1^\circ \times 1^\circ$ grid box. **b-1** shows the average of $Z_e \geq 40$ dBZ when Z_e is considered as convective pixels using TRMM 2A23 data. **a-2, b-2** are similar to **(a-1, b-1)** but now for the stratiform pixels. Numbers in colour bar are count **(a-1, a-2)** and dBZ **(b-1, b-2)**



that less than 10 % of the bright band consists of $Z_e \geq 40$ dBZ, whereas the Bay has only 5 % of the bright band with $Z_e \geq 40$ dBZ.

3.2 Definition of subregions

The selected regions are based on previous studies and on $Z_e \geq 40$ dBZ statistics. Figure 1 shows the climatology of the spatial distribution of rainfall during JJAS, and Fig. 3 shows the statistics of $Z_e \geq 40$ dBZ observed from TRMM PR. Ten

regions are selected for inter-comparison in the vertical structure of convective clouds. R-1 is the area characterized by the midtropospheric cyclones (Miller and Keshavamurthy 1968), whereas areas R-3 and R-4 are part of main monsoon zone. Two boxes are selected in the western regions, one in the Arabian Sea (R-2) and the other around the Western Ghats (R-7). One of the main aims is to understand the difference in the vertical structure of the most intense convective clouds over the Arabian Sea and the Bay. R-6 and R-8 are the regions in the Bay of Bengal that are highly convective (Goswami et al. 2003). The box over the Western Ghats (R-7) is characterized by the orographic lifting which produces heavy precipitation. R-9 and R-10 are the areas in the equatorial oceans.

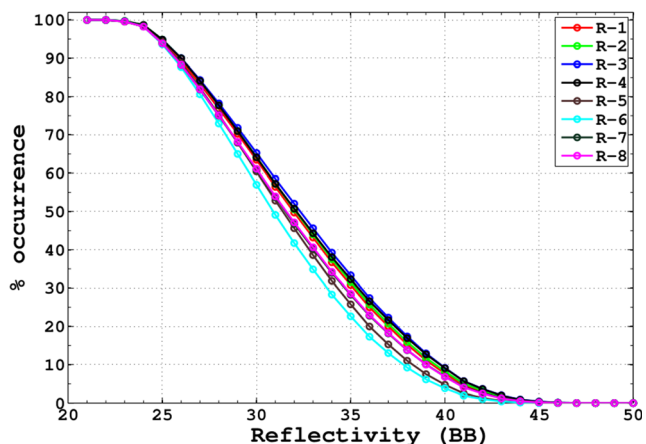


Fig. 4 Intensity of bright band observed from TRMM. Bright bands with $Z_e \geq 40$ dBZ are less than 10 % over Indian regions. Over BOB, it is less than 5 %

3.3 Definition of MICC

Vertical profile of maximum reflectivity (Z_e) within a cloud system is a strong indicator of storm type (e.g. Zipser and Lutz 1994; Xu and Zipser 2012). The life cycle of MCS consists of the growing, mature and decaying stages, and the mature stage has the highest reflectivity values during the life cycle (Williams et al. 1989). Reflectivity values higher than 40 and 35 dBZ at 4.4 and 3.9 km, respectively, were used for defining convective clouds over midlatitude and tropical systems (Zipser and Lutz 1994). Selecting $Z_e \geq 40$ dBZ as a threshold for convective clouds, based on previous studies, does not look like an appropriate choice, as shown in Figs. 3

and 4. The values of $Z_{e \geq 40}$ dBZ also correspond to the melting band (bright band) and stratiform precipitation. Hence, TRMM 2A23 is used to exclude the stratiform clouds from the present analysis. First, the convective pixels from the TRMM 2A23 are selected, and then, MICC is derived. MICC consists of the maximum Z_e value at each altitude within the population of convective clouds, with at least one convective pixel higher than 40 dBZ. The lateral size of cloud pixels is equal to the radar horizontal size. It is important that different pixels at all altitude should be connected. Different pixels of MICC correspond to different mature convective cells present at the time of observation. An additional study (not shown) shows that for most of the MICC, ~75–80 % of pixels of each MICC come from the nearest pixels of maximum Z_e (i.e. Fig. 2). So, most of the pixels (at different altitude) of each MICC are connected, and MICCs show an important aspect of convective clouds. Also, there are few vertical profiles in which observed reflectivity values are below the PR detection threshold value (~17 dBZ) at some altitude with higher values at higher altitude. To avoid such cases, only those vertical profiles are considered, where at least four pixels are higher than 17 dBZ; the altitude with Z_e is less than 17 dBZ. Also, MICCs with less than 1.5-km width are not considered in the present study, which are very shallow clouds. The present study finds the regional differences between the Indian land and surrounding oceans. We also separate the MICCs, whose tops cross the 10 km (i.e. deep clouds) and 15 km (near the upper level of tropopause).

4 Results

In the region under study (Fig. 3), around ~14,000 MICCs occurred over the period of 10 years (2001–2010) during June–September. Table 2 shows the number of individual MICCs occurring in the present study over different areas. The Indo-Gangetic plain (R-3 and R-4) exhibits a higher number of MICCs, whereas R-1 has the least number of MICC. The individual vertical profile of MICCs (R-1 and R-4; supplementary figure 1) shows the common features. In the majority of cases, Z_e decreases rapidly above 6 km. Some active clouds do not cross the 5-km altitude, whereas some intense convective clouds go beyond the 17 km altitude (discuss later).

4.1 Top height distribution

Figure 5 shows the MICC top height distribution (see the figure caption for definition). Figure 5a shows the frequency of MICC occurrence within each 2-km height interval, and Fig. 5b shows the cumulative frequency distribution of the MICC top height. Cloud top height with below 6 km and above 18 km shows higher regional differences (Fig. 5).

Table 2 Total number of individual profiles in selected regions for JJAS during last 10 years. Top height distribution of MICC (in %) at different altitude (km) in different regions

Regions	No. of MICC	MICC \leq 5 km	MICC \geq 15 km	MICC \geq 18 km
R-1	984	20.5	14.6	1.2
R-2	1617	16.6	1.9	0.4
R-3	2099	1.9	30.2	3
R-4	2678	1	28.6	2.1
R-5	1580	4.8	19.2	1
R-6	1769	5.8	10.2	0.4
R-7	1062	12.7	4	0.5
R-8	971	6.6	15.6	0.9
R-9	506	20.3	1.8	0
R-10	732	6.9	7.7	0.3

Land-dominated areas (R-3, R-4 and R-5) show a higher frequency (≥ 20 –30 %; Table 2) of MICCs above the 15-km altitude. The western side of India (R-2, R-7 and R-9) has a higher frequency of low-level clouds. Cumulative distribution of MICCs show that nearly 30 % of MICCs are crossing the 15-km altitude over the Indo-Gangetic plain (R-3 and R-4), whereas only ~2 % MICCs are crossing the 15-km altitude over R-2 (Arabian Sea) and R-9 (near equatorial ocean). Nearly 4 % of MICCs are crossing the 15-km altitude over the Western Ghats. Nearly 65 % of MICCs are crossing the 10-km altitude over the Indo-Gangetic plain, whereas only 20 % of MICCs are crossing the 10-km altitude over R-2 (Arabian Sea). Land-originated CCN and higher convective available potential energy (CAPE) over land delay the precipitation over R-3 and R-4. The western and eastern equatorial Indian Oceans show different characteristics, as the west has a higher fraction (%) of warm clouds. The overall summary of cloud top height distribution is given in Table 2

4.2 Average vertical profile

Figure 6 shows the average vertical profiles of MICCs. The average profile is calculated by using the condition that at least 10 % data points should be at each height, and average is considered for altitudes above 1.5 km for removing the near ground clutter. This condition is imposed because the number of data points is too little at higher altitudes compared to lower altitudes (supplementary figure 1). The strongest Z_e profile is observed in R-3, R-4 (Indo-Gangetic plain) and R-5 (central India), which are mainly land-dominated areas. The highest value of average Z_e corresponds to R-3 (i.e. part of the main monsoon zone on land) at all altitudes, whereas R-2 (Arabian Sea), R-7 (Western Ghats) and R-9 (IOW) show the lowest Z_e above and below 10-km altitude. The peaks in Z_e occur around the ~2.25-km height over the

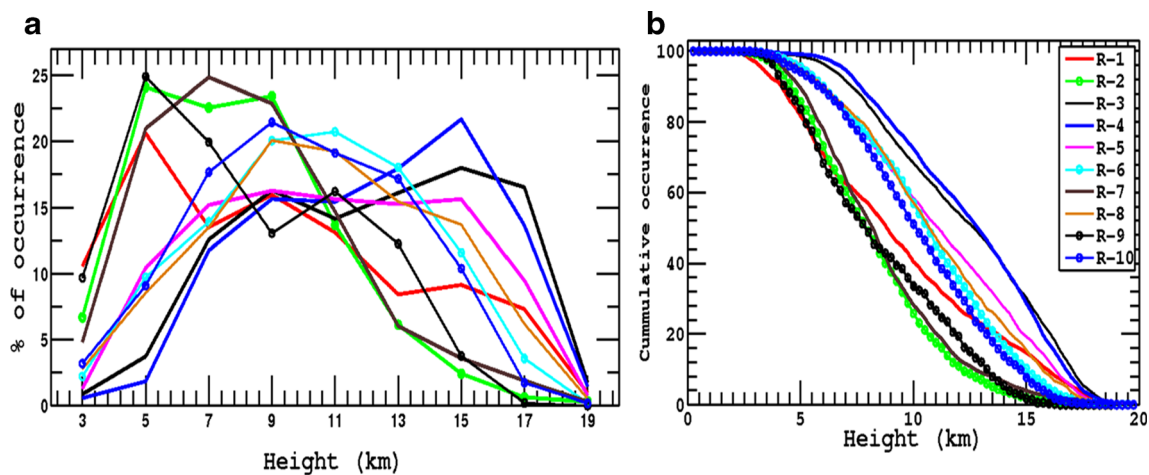


Fig. 5 **a** Frequency and **b** cumulative frequency distribution of cloud top height distribution. The cloud top height is calculated by using the maximum height of 17 dBZ. The x -axis is height and the frequency is calculated at each 2-km interval, i.e. 3 km means the MICC lies between 2 and 4 km (**a**)

Arabian Sea (R-2) and Western Ghats (R-7), and the rate of its decrease is rapid above 3 km, i.e. the decreasing trend begins well below the freezing level (which is about 5-km height; Saikranthi et al. 2013). For land-dominated areas (R-3, R-4 and R-5), the peak occurs around 4.25 km and then decreases rapidly. Regional differences are more pronounced in the 5- to 12-km altitude range and show the effect of mixed-phase dynamics (Heymsfield et al. 2010; Xu and Zipser 2012). The Ze profile over R-1 matches with

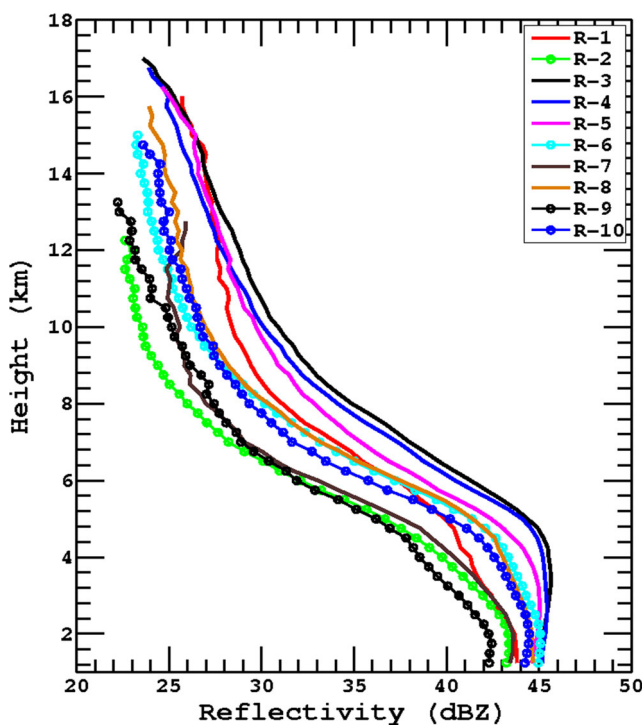


Fig. 6 Average vertical profile for MICC. The average is calculated by considering 90 % of data points at each altitude. Data below 1.5 km is also removed because of ground clutter

that over the Arabian Sea (R-2) and Western Ghats (R-7) below 4 km and compares with R-3 and R-4 (land areas) above 12 km and represents the proxy for land and ocean. The least vertical extension occurs over the Arabian Sea (R-2), equatorial ocean (R-9) and Western Ghats (R-7), where the average is well below 14 km, compared to land-dominated areas, where the average is crossing the 16-km altitude.

The average vertical profile of MICCs, which are crossing 10 and 15 km, shows the reverse behaviour (Fig. 7) compared to Fig. 6. The Western Ghats (R-7) shows the highest value above the 15-km altitude (Fig. 7b). The Western Ghats (R-7) and central India (R-5) show the strongest vertical profile (contains higher Ze) compared to R-3 and R-4 (Indo-Gangetic plain). Land versus ocean differences vanish for the convective clouds, when they cross the 10-km altitude. This indicates that the mixed-phase height regions are important when considering the vertical structure of the convective clouds (Xu and Zipser 2012). Oceanic regions near the areas (Bay and Arabian Sea) show almost similar patterns (Fig. 7b) compared to Fig. 6. The western equatorial Indian Ocean (R-9) shows the weakest vertical profile. Table 2 shows that the number of MICCs crossing the 15 km is less, but they are more intense in the Western Ghats (Fig. 7). In all cases, higher regional differences occur between the 5- and 12-km altitudes and lower differences occur below the 4-km altitude.

4.3 Precipitation structure of MICC

Figure 8 shows the contour frequency by altitude diagram (CFAD; Yuter and Houze 1995) of MICCs that shows the frequency-altitude dependence. For constructing the CFAD diagram, first the number of occurrences of Ze in each 1 dBZ interval from 17 to 60 dBZ and at each 0.25 km (vertical) is

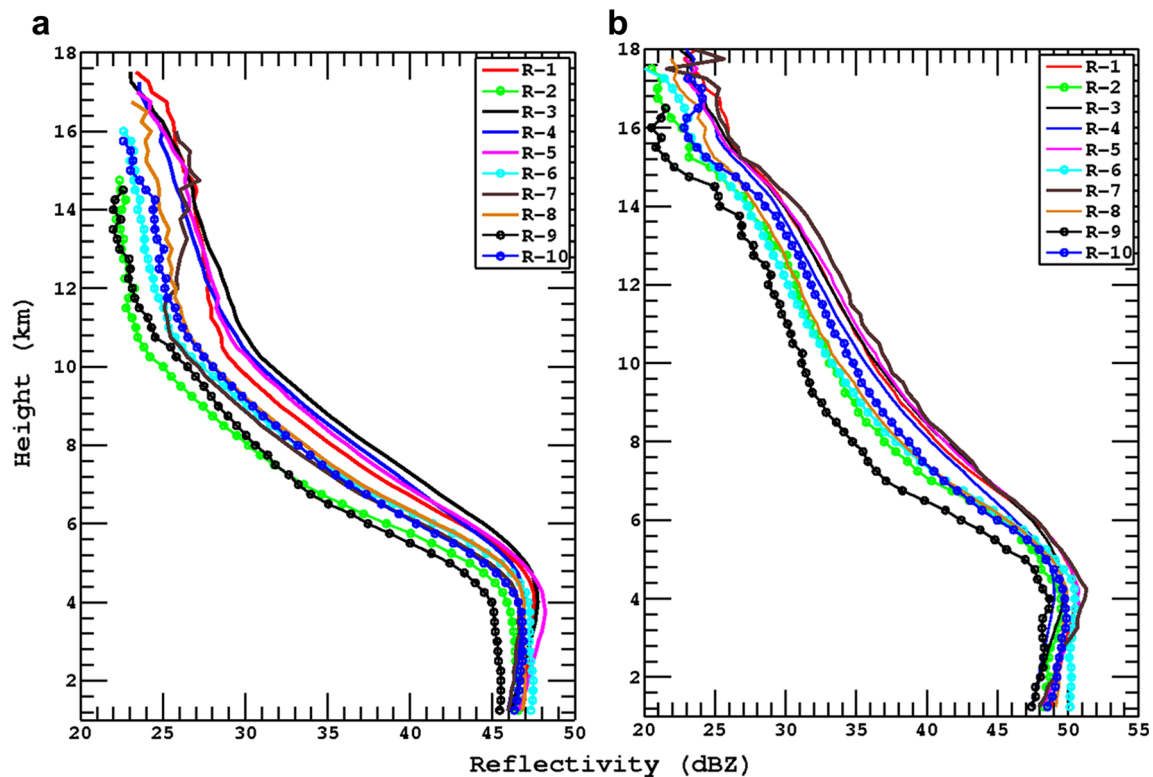


Fig. 7 a, b Average vertical profile of Ze for MICC crossing 10 and 15 km. The average is calculated by considering that at least 90 % of data must contribute at each altitude. Data below 1.5 km is removed because of ground clutter

calculated. The number of occurrence at each height interval, $f(\text{dBZ}, \text{Hgt})$, is normalized by the $f_{\text{max}}(\text{dBZ}, \text{Hgt})$. $f(\text{dBZ}, \text{Hgt}) \leq 10$ is eliminated from the entire volume. The CFAD is divided into two regions, below and above 0°C (near-freezing level). Below 0°C , the CFADs are broad and suggest the higher precipitation intensity and are mainly produced by bigger raindrops. Above 0°C , CFAD shows the lower reflectivity values and indicates weaker precipitation at higher altitude.

Below 5 km, the mode for MICCs occurs around 40–45 dBZ for all the subareas, with different vertical extension. The maxima over the land areas (R-3, R-4, R-5) and Bay (R-6 and R-8) reach up to 5 km, whereas over other subareas, they are just below 3 km. CFAD for MICCs show the decreasing trend of reflectivity between 5 and 8 km. The width of CFAD below 0°C shows that convection is intense and higher over land areas compared with oceanic areas. Above 10 km, the higher width in CFAD for land areas shows the substantial variation in Ze. CFAD for the oceanic regions show less width compared to the land-dominated areas, which indicates the weak intense precipitation.

4.4 Proxy of convective intensity

Figure 9 shows the maximum height of 30 and 40 dBZ (MH30 and MH40). In the absence of the vertical velocity, MH30 and MH40 are used as the proxy for the convective

intensity (Zipser et al. 2006; Xu and Zipser 2012; Bhat and Kumar 2015). The Indo-Gangetic plain (R-3 and R-4) shows the highest fraction (25 percentile) of MICC above 8 km (MH40) altitude, whereas the corresponding value for MH30 is 12 km. The western side (R-1, R-2, R-7 and R-9) shows the least fraction of MH30 and MH40. Fifty percent of MH40 and MH30 are crossing 6.5 and 8.5 km near the Indo-Gangetic plain, respectively, whereas the corresponding height over the Western Ghats is 4.5 and 6 km, respectively.

5 Discussion

Ze is a proxy for hydrometeor concentration and its size. Several factors such as strength of low-level convergence, vertical velocity (updraft and downdraft) inside the cloud and horizontal wind shear influence the vertical distribution of hydrometeors. Falling hydrometeors below the freezing level contribute to the precipitation locally and affect the cloud properties. Precipitation formation is a complex process, and several microphysical processes are involved. Microphysical processes are strongly affected by the altitude and phase of hydrometeors.

The difference between R-4 and R-8 appears to be the classic case of continental versus oceanic clouds (Nesbitt et al. 2000; Toracinta et al. 2002; Liu et al. 2007). In Fig. 6,

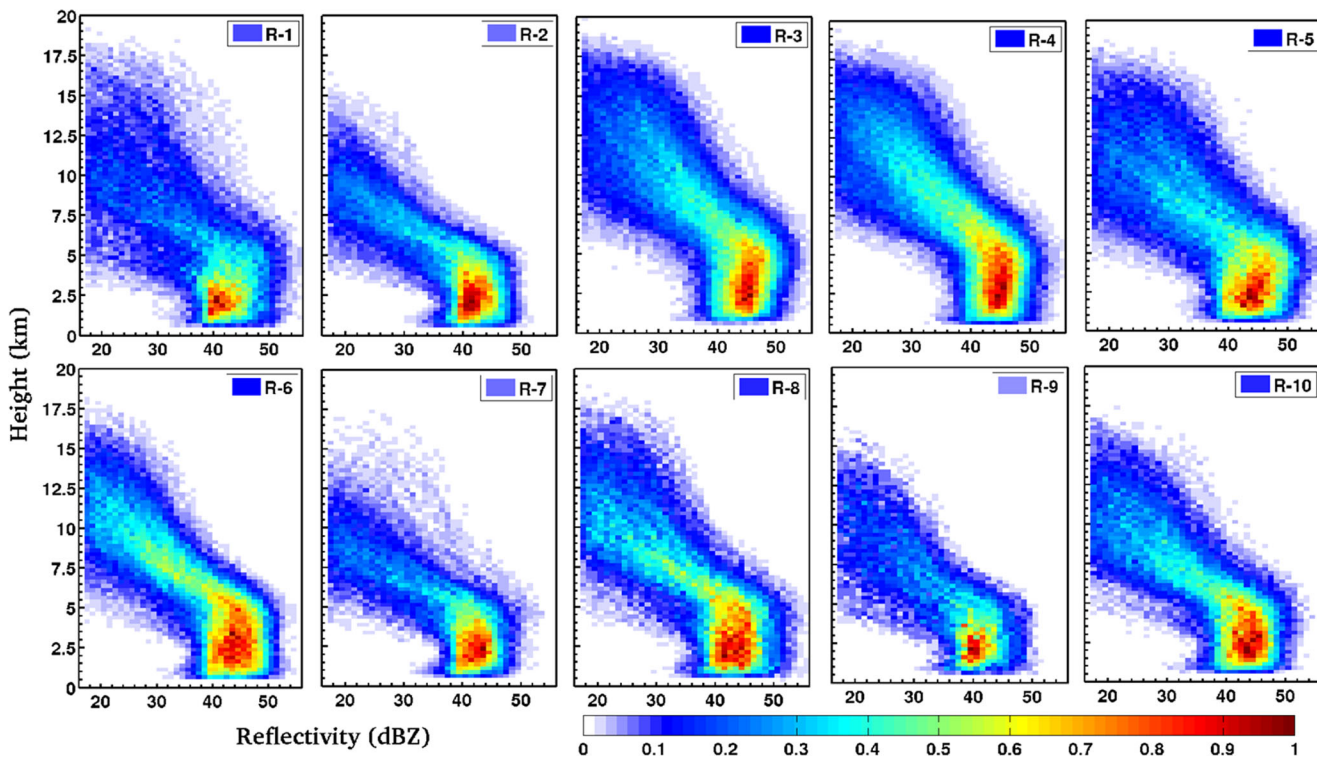


Fig. 8 Contour frequency by altitude diagram (CFAD) for the MICC. Number of occurrence in each reflectivity bin from 18 to 60 dBZ at 1 dBZ and 0.25-km interval is calculated. The image shows the % of occurrence in each x-y bin

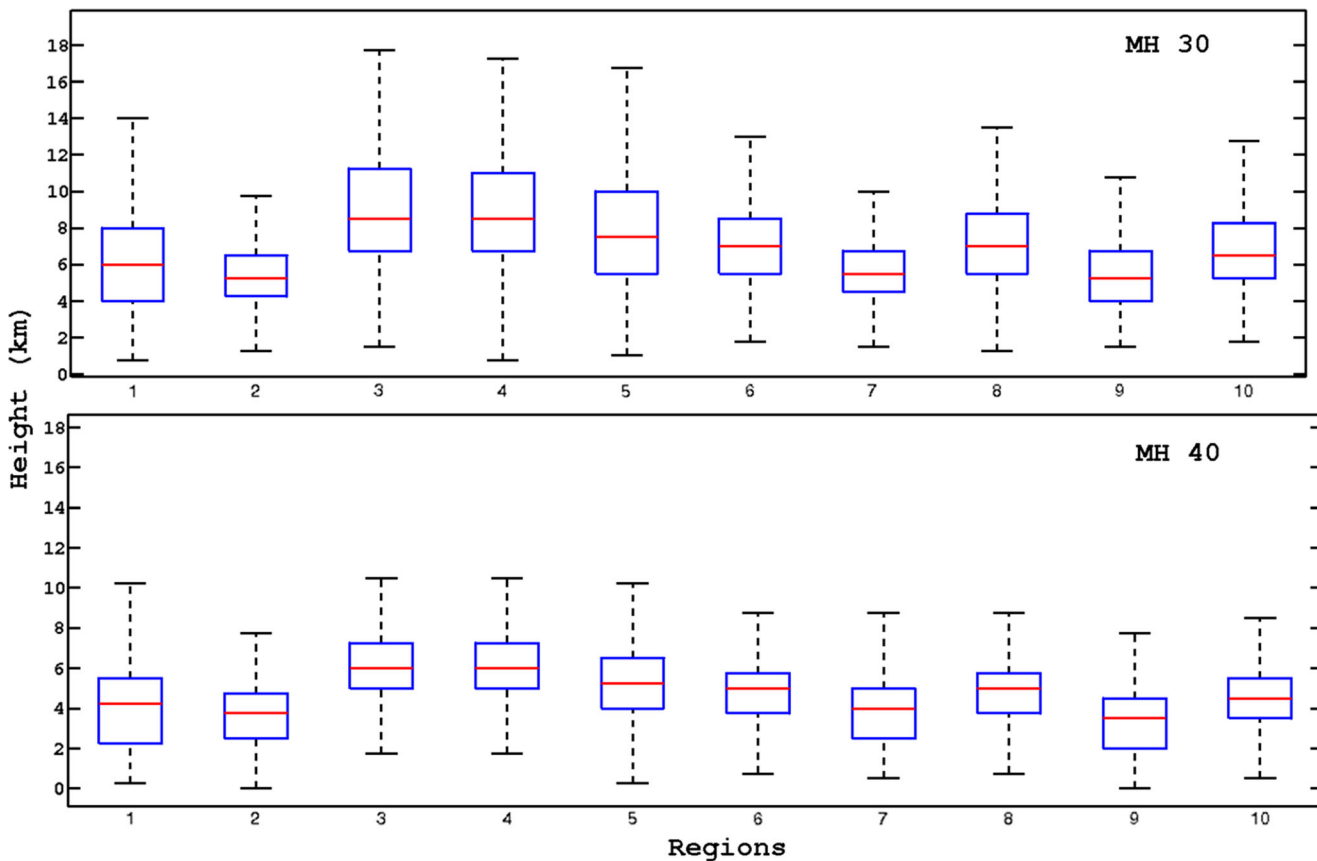
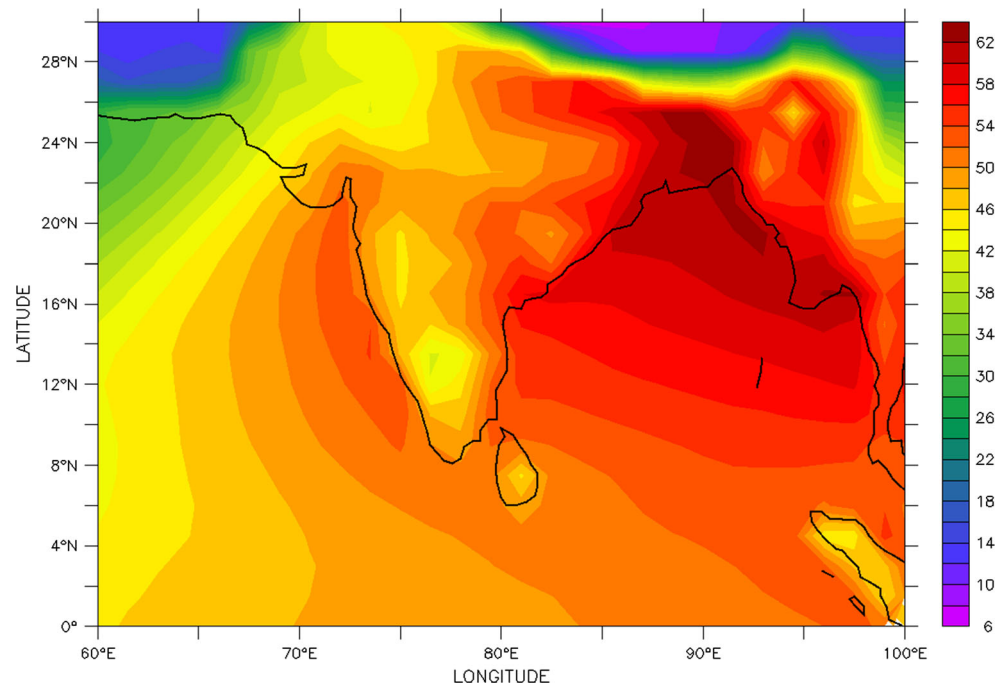


Fig. 9 Maximum height of 40 and 30 dBZ. Red colour shows the median value whereas the lower and upper boundary of boxes is showing the 75 and 25 percentiles of maximum height

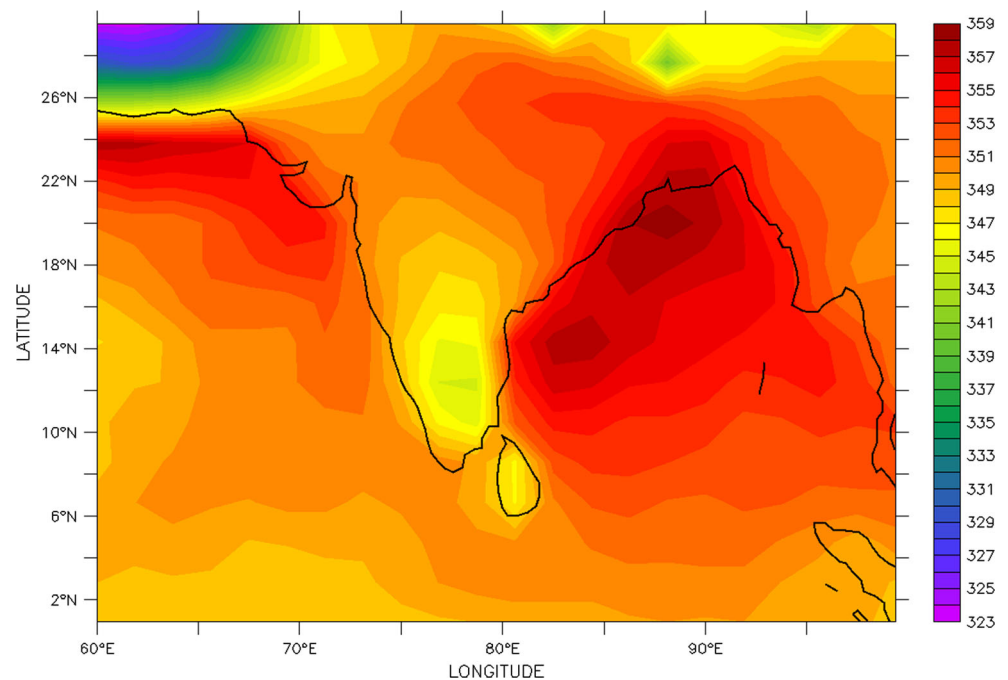
Fig. 10 Column water vapour from NCEP data, averaged for 10 years (2001–2010) for the months of JJAS. Unit is in kg m^{-2}



Z_e values in R-3 and R-4 areas are nearly 10 dBZ higher compared to that over the Arabian Sea (R-2) and Western Ghats (R-7). Higher differences between 5 and 12 km (Figs. 6 and 7) reveal that mixed-phase dynamics play an important role in the vertical structure (Heymsfield et al. 2010; Xu and Zipser 2012). Reflectivity (Z_e) differences are less, when we consider the $\text{MICC} \geq 10$ km and least for the

$\text{MICC} \geq 15$ km. The different microphysical processes, such as riming and deposition, depend on the altitude. A small change in the vertical velocity causes the higher differences in reflectivity values within the mixed-phase regions (Heymsfield et al. 2010). Higher reflectivity above the freezing level indicates the strong updraft speed and large ice particles over the land areas (Zipser and Lutz 1994; Zipser et al. 2006). Going

Fig. 11 Surface moist static energy based on NCEP reanalysis data. Unit is in KJ kg^{-1}



by experience, land areas show stronger updrafts and higher CAPE, which stimulate the large-size hydrometeors at high altitude (Lucas et al. 1994).

Development of a precipitating cloud requires a moist surrounding environment, as precipitating clouds do not develop in dry surrounding air (Sherwood et al. 2004). Moist static energy (MSE) is an important parameter for moist convection, as MSE relates the thermodynamic properties, such as temperature and specific humidity in one equation as $h = C_p * T + L_v * q + g * Z$, where h is MSE, C_p is the specific heat of air at constant pressure, T the temperature, g acceleration due to gravity, Z the height above mean sea level, L latent heat of evaporation of water and q the mass of water vapour per unit mass of moist air, i.e. specific humidity. Spatial distribution of column water vapour (Fig. 10), MSE (Fig. 11) and vertical distribution of MSE (Fig. 12) using NCEP data are shown. Due to weak temperature gradients (Sobel and Bretherton 2000) in the tropics, a lower MSE in the midtroposphere points to a drier air. The Bay (R-8) shows the highest MSE at the surface and a relatively more moist midtroposphere (Fig. 11). The western coast of India shows relatively less surface specific humidity and its midtroposphere is also drier. This may partially explain why R-2, R-7 and R-9 show smaller reflectivity values. Land and ocean differences also arise due to the type of CCN and moisture availability (e.g. Rosenfeld et al. 2008). Oceanic regions have a lower concentration of CCN, which is dominated by salt particles

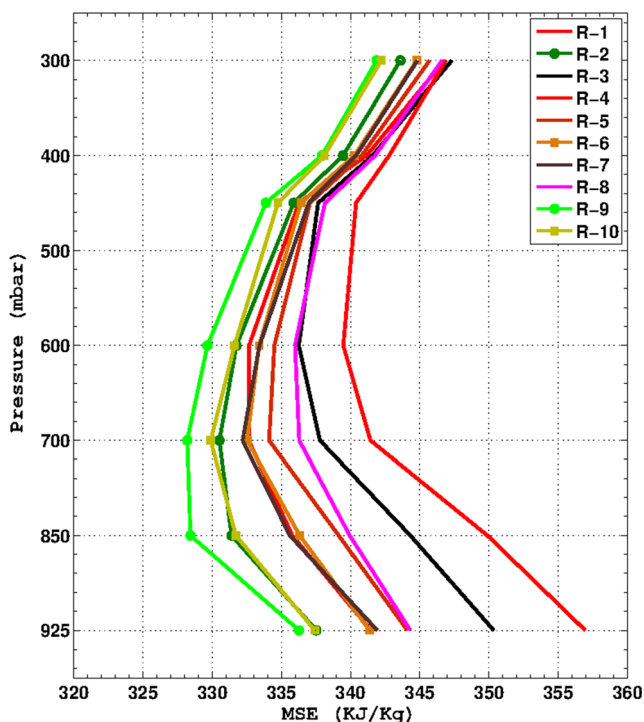


Fig. 12 Vertical profile of moist static energy (MSE) for JJAS months of 2001–2010 based on NCEP data. Unit is in KJ kg^{-1}

(Pruppacher and Klett 1997), that favours the warm rain processes and leaves fewer hydrometeors to carry at higher altitude (Konwar et al. 2012). Over land, precipitation is delayed due to a higher concentration of CCN (Rosenfeld et al. 2008; Konwar et al. 2012), and more water is carried to higher levels (e.g. Wang 2005).

The average vertical profile and cloud top height distribution over the Arabian Sea (AS; R-2) and Bay of Bengal (BOB; R-6) show how different surface and atmospheric conditions (horizontal pattern and vertical profile of MSE, water vapour) influence the cloud properties. Below the freezing level, number of MICCs are higher (i.e. $\sim 16\%$) over R-2 compared to R-6 ($\sim 5.8\%$). The difference in MSE (Figs. 11 and 12) over AS and BOB is because of the difference in q , as SST does not show much difference. The Arabian Sea is more saline, and the CCN over AS is dominated by salt particles. Over the Arabian Sea, giant CCNs favour early precipitation formation by the collision-coalescence mechanism (Konwar et al. 2012). As a result, condensed water is removed nearer to the cloud base in Arabian Sea clouds compared to Bay clouds.

6 Conclusions

The objective of the present paper is to understand reflectivity distribution in the most intense convective clouds and regional differences between the east and west coast of India. Understanding vertical structure of reflectivity is important as it reflects the distribution of the hydrometeors within the convective clouds. The most intense convective cell is constructed from the population of convective clouds for ten distinct areas over the Indian region by using TRMM 2A23 and 2A25 data. The following are the major conclusions of the study:

1. The differences in the vertical profile are higher between 5- and 12-km altitudes, and land cells are more intense as compared to ocean cells. Land versus ocean separations becomes less in deep convective clouds (i.e. MICCs are crossing 10 km) and least when MICCs are crossing the 15-km altitude. The regional differences in Z_e depend on the cloud top height of MICC.
2. On an average, clouds over the Indo-Gangetic plain are more intense (shows higher reflectivity values), whereas the Arabian Sea and Indian Ocean near the equator (west side) have the weakest convective clouds. The Western Ghats has less fraction of MICC (>15 km), but they are the most intense clouds.
3. West versus east differences in Z_e and cloud top height are clear, and average vertical profiles are stronger (high Z_e) near the eastern coast/side compared to the western coast/side and have a higher fraction of high-level clouds.

References

- Alcala C, Dessler A (2002) Observations of deep convection in the tropics using the tropical rainfall measuring mission (TRMM) precipitation radar. *J Geophys Res* 107:D244792. doi:10.1029/2002JD002457
- Awaka J, Iguchi T, Okomoto K (2009) TRMM PR standard algorithm 2A23 and its performance on bright band detection. *J Meteorol Soc Jpn* 87A:31–52
- Bhat GS, Kumar S (2015) Vertical structure of cumulonimbus towers and intense convective clouds over the South Asian region during the summer monsoon season. *J Geophys Res Atmos*. doi:10.1002/2014JD022552
- Charney JG (1969) A further note on large-scale motions in the tropics. *J Atmos Sci* 26:182–185
- Dixon M, Wiener G (1993) TITAN: thunderstorm identification, tracking, analysis, and nowcasting a radar-based methodology. *J Atmos Oceanic Tech* 10:785–797
- Goswami BN, Ajayamohan R, Xavier PK, Sengupta D (2003) Clustering of synoptic activity by Indian summer monsoon intraseasonal oscillations. *Geophys Res Lett* 30:141–144. doi:10.1029/2002GL016734
- Heymsfield GM, Tian L, Heymsfield AJ, Li L, Guimond S (2010) Characteristics of deep tropical and subtropical convection from nadir-viewing high-altitude airborne Doppler radar. *J Atmos Sci* 67:285–308
- Hirose K, Nakamura K (2005) Spatial and diurnal variation of precipitation systems over Asia observed by the TRMM precipitation radar. *J Geophys Res* 110: doi:10.1029/2004JD004815
- Holton JR (2004) An introduction to dynamic meteorology, Chapter 11; 4th Edition. Elsevier Academic Press, New York, pp 531
- Houze RA Jr (1989) Observed structure of mesoscale convective system and implications for large-scale heating. *Q J Roy Meteorol Soc* 115: 425–461
- Houze RA Jr, Wilton DC, Smull FB (2007) Monsoon convection in the Himalayan region as seen by the TRMM precipitation radar. *Q J Roy Meteorol Soc* 133:1389–1411
- Huffman GJ, Coauthors (2007) The TRMM Multisatellite Precipitation Analysis (TMPA): Quasi-Global, Multilayer, Combined-sensor Precipitation Estimates at Fine Scales. *J Hydrometeor* 8:38–55
- Iguchi T, Kozu T, Meneghini R, Awaka J, Okamoto K (2000) Rain-profiling algorithm for the TRMM precipitation radar. *J Appl Meteorol* 39:2038–2052
- Kalnay E et al (1996) The NCEP/NCAR 40 year reanalysis project. *Bull Am Meteorol Soc* 77:437–470
- Konwar M, Maheskumar RS, Kulkarni JR, Freud E, Goswami BN, Rosenfeld D (2012) Aerosol control on depth of warm rain in convective clouds. *J Geophys Res* 117: doi:10.1029/2012JD017585
- Kummerow C, Barnes W, Kozu T, Shiue J, Simpson J (1998) The tropical rainfall measuring mission (TRMM) sensor package. *J Atmos Oceanic Tech* 15:809–817
- Kummerow C, Simpson J, Thiele O, Barnes W, Chang ATC, Stocker E, Adler RF, Hou A, Kakar R, Wentz F, Ashcroft P, Kozu T, Hong Y, Okamoto K, Iguchi T, Kuroiwa H, Im E, Haddad Z, Huffman G, Ferrier B, Olson WS, Zipser E, Smith EA, Wilhelm TT, North G, Krishnamurti T, Nakamura (2000) The status of the tropical rainfall measuring mission (TRMM) after two years in orbit. *J Appl Meteorol* 39:1965–1982
- Li W, Schumacher C (2011) Thick anvils as viewed by the TRMM precipitation radar. *J Climate* 24:1718–1735
- Liu C, Zipser ED, Nesbitt SW (2007) Global distribution of tropical deep convection: different perspectives from TRMM infrared and radar data. *J Climate* 20:489–503
- Liu C, Zipser ED, Cecil SW, Nesbitt SW, Sherwood S (2008) A cloud and precipitation feature database from nine years of TRMM observations. *J Appl Meteorol Climatol* 47(10):2712–2728
- Liu C, Cecil DJ, Zipser EJ, Kronfeld K, Robertson R (2012) Relationships between lightning flash rates and radar reflectivity vertical structures in thunderstorms over the tropics and subtropics. *J Geophys Res* 117: D06212. doi:10.1029/2011JD017123
- Lucas C, Zipser EJ, LeMone MA (1994) Vertical velocity in oceanic convection off tropical Australia. *J Atmos Sci* 51:3183–3193
- Masunaga H, Iguchi T, Oki R, Kachi M (2002) Comparison of rainfall products derived from TRMM microwave imager and precipitation radar. *J Appl Meteorol* 41:849–862
- Medina S, Houze RA Jr, Kumar A, Niyogi D (2010) Summer monsoon convection in the Himalayan region: terrain and land cover effects. *Quart J Roy Meteor Soc* 136:593–616
- Miller FR, Keshavamurthy RN (1968) Structure of an Arabian sea summer monsoon system. East West Center Press, Honolulu
- Nesbitt SW, Zipser E, Cecil C (2000) A census of precipitation features in the tropics using TRMM radar, ice scattering, and lightning observations. *J Climate* 13:4087–4106
- Nesbitt SW, Cifelli R, Rutledge A (2006) Storm morphology and rainfall characteristics of TRMM precipitation features. *Mon Weather Rev* 134:2702–2721
- Pruppacher HR, Klett JD (1997) Microphysics of clouds and precipitation. Kluwer Academic Publishers, Dordrecht, p 961
- Rao YP (1976) Southwest monsoon. India Meteorological Department. http://www.imd.gov.in/section/nhac/dynamic/Monsoon_frame.html
- Riehl H (1979) Climate and weather in the tropics. Academic Press, London, p 611
- Romatschke U, Houze RA Jr (2011a) Characteristics of precipitating convective systems in the premonsoon season of South Asia. *J Hydrometeorol* 12:3–26. doi:10.1175/2010JHM1289
- Romatschke U, Houze RA Jr (2011b) Characteristics of precipitating convective systems in the South Asian Monsoon. *J Hydrometeorol* 12:157–180. doi:10.1175/2010JHM1311.1
- Romatschke U, Medina S, Houze RA Jr (2010) Regional, seasonal, and diurnal variations of extreme convection in South Asian region. *J Climate* 23:419–439
- Rosenfeld D, Lohmann U, Raga GB, O'Dowd CD, Kulmala M, Fuzzi S, Reissell A, Andreae MO (2008) Flood or drought: how do aerosols affect precipitation? *Science* 321:1309–1313
- Rosenfeld D, William LW, Khain A, Cotton WR, Carrio G, Ginis I, Golden JH (2012) Aerosol effects on microstructure and intensity of tropical cyclones. *Bull Am Meteorol Soc* 93:987–1001
- Saikranthi K, Narayana TN, Radhakrishna B, Rao SVB (2013) Impact of misrepresentation of freezing-level height by the TRMM Algorithm on shallow rain statistics over India and adjoining oceans. *J Appl Metroe Clim* 52: 2001:2008
- Saikranthi K, Narayana TN, Radhakrishna B, RAO SVB (2014) Morphology of the vertical structure of precipitation over India and adjoining oceans based on long-term measurements of TRMM PR. *Geophys Res Atmos* 119:8433–8449. doi:10.1002/2014JD021774
- Sherwood SC, Minnis P, McGill M (2004) Deep convective cloud-top heights and their thermodynamic control during crystal-face. *J Geophys Res* 109: doi:10.1029/2004JD004811
- Simpson J, Kummerow C, Tao W, Adler R (1998) Eyeing the eye: exciting early stage science results from TRMM. *Bull Am Meteorol Soc* 79:1711–1711
- Sobel A, Bretherton CS (2000) Modeling tropical precipitation in a single column. *J Climate* 13:4378–4392
- Steiner M, Houze RA, Yuter SE (1995) Climatological characterization of three-dimensional storm structure from operational radar and rain gauge data. *J Appl Meteorol* 34:1978–2007

- Takayabu YN (2002) Spectral representation of rain profile and diurnal variations observed with TRMM PR over the equatorial area. *Geophys Res Lett* 29: doi:[10.1029/2001GL014113](https://doi.org/10.1029/2001GL014113)
- Toracinta E, Cecil D, Zipser E, Nesbitt S (2002) Radar, passive microwave, and lightning characteristics of precipitating systems in the tropics. *Mon Weather Rev* 130:802–824. doi:[10.1175/1520-0493](https://doi.org/10.1175/1520-0493)
- Wang C (2005) A modeling study of the response of tropical deep convection to the increase of cloud condensation nuclei concentration: 1. Dynamics and microphysics. *J Geophys Res* 110: doi:[10.1029/2004JD005720](https://doi.org/10.1029/2004JD005720)
- Williams ER, Weber ME, Orville RE (1989) The relationship between lightning type and convective state of thunderstorms. *J Geophys Res* 94:13213–13220
- Xu W, Zipser EJ (2012) Properties of deep convection in tropical continental, monsoon, and oceanic rainfall regimes. *Geophys Res Lett* 39: doi:[10.1029/2012GL051242](https://doi.org/10.1029/2012GL051242)
- Yuter SE, Houze RA Jr (1995) Three-dimensional kinematic and microphysical evolution of Florida cumulonimbus. Part II: frequency distribution of vertical velocity, reflectivity, and differential reflectivity. *Mon Weather Rev* 123:1941–1963
- Zipser EJ, Lutz K (1994) The vertical profile of radar reflectivity of convective cells a strong indicator of storm intensity and lightning probability. *Mon Weather Rev* 122:1751–1759
- Zipser EJ, Cecil DJ, Liu C, Nesbitt SW, Yorty DP (2006) Where are the most intense thunderstorms on Earth? *Bull Am Meteorol Soc* 87: 1057–1071